Atmospheric Environment 358 (2025) 121341

Contents lists available at ScienceDirect

Atmospheric Environment

journal homepage: www.elsevier.com/locate/atmosenv

The broadband light analyzer of complex aerosol: characterization and first applications

Tommaso Isolabella [a,b], Marco Brunoldi [a,b], Federico Mazzei [a,b,*], Franco Parodi [b], Paolo Prati [a,b], Virginia Vernocchi [b], Vera Bernardoni [c,d], Gianluigi Valli [c,d], Roberta Vecchi [c,d], Paola Formenti [e], Clarissa Baldo [f,g], Mathieu Cazaunau [f], Vaios Moschos [h], Solomon Bililign [h], Marc N. Fiddler [h], Dario Massabò [a,b]

[a] Dipartimento di Fisica, Università di Genova, Genoa, Italy
[b] Istituto Nazionale di Fisica Nucleare (INFN), Sezione di Genova, Genoa, Italy
[c] Dipartimento di Fisica, Università degli Studi di Milano, Milan, Italy
[d] Istituto Nazionale di Fisica Nucleare (INFN), Sezione di Milano, Milan, Italy
[e] Université Paris Cité and Univ Paris Est Creteil, CNRS, LISA, F-75013, Paris, France
[f] Univ Paris Est Creteil and Université Paris Cité, CNRS, LISA, F-94010, Créteil, France
[g] now at Université Paris Cité and Univ Paris Est Creteil, CNRS, LISA, F-75013, Paris, France
[h] Department of Physics, College of Science and Technology, North Carolina A&T State University, United States

HIGHLIGHTS

- We present a new laboratory instrument for aerosol light absorption measurements.
- The absorption is measured offline between 375 and 1000 nm with a 5 nm resolution.
- A wide range of loadings and aerosol types can be analyzed.
- The instrument achieved up to 99 % accuracy in validation campaigns.

GRAPHICAL ABSTRACT

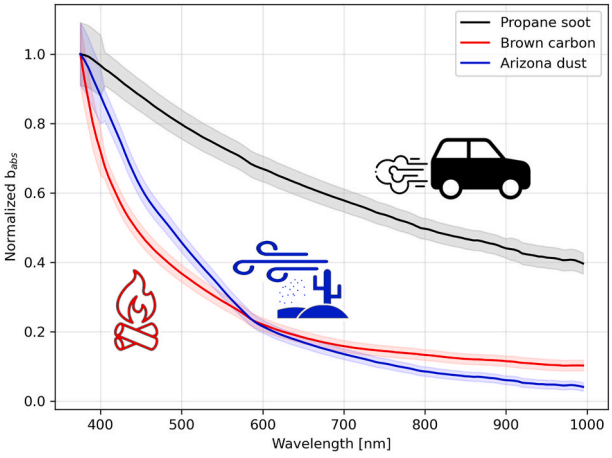

ABSTRACT

We introduce a new instrument to measure spectral light absorption by aerosol particles. BLAnCA (Broadband Light Analyzer of Complex Aerosol) is an automatic laboratory instrument for offline measurement of aerosol collected on suitable media. BLAnCA is equipped with a white light source and a high-resolution spectrometer, and measures in the range between 375 and 1000 nm with a spectral resolution of 5 nm. This allows for the determination of fine structure of the absorption properties of a sampled aerosol, which can lead to improvement in the robustness and scope of source apportionment and the evaluation of climate-relevant

* Corresponding author. Dipartimento di Fisica, Università di Genova, Genoa, Italy.
E-mail address: fmazzei@ge.infn.it (F. Mazzei).

https://doi.org/10.1016/j.atmosenv.2025.121341
Received 3 December 2024; Received in revised form 3 June 2025; Accepted 7 June 2025
Available online 9 June 2025

properties such as the aerosol mass absorption cross-section. The new instrument has been validated against a multi-wavelength absorbance analyzer, obtaining an agreement of up to 99 % between absorption coefficient measurements. The absorption coefficient limit of detection for BLAnCA has been estimated at 1.20 Mm^{-1} (2.70 Mm^{-1}) for standard EU (EPA) sampling conditions, corresponding to an elemental carbon detection limit of about 1.3 $\mu g\ cm^{-2}$, if a mass absorption cross-section of 4.7 m^2g^{-1} at 1000 nm is considered. The instrument has been used to characterize several types of aerosol samples, each with its own distinct absorption features, which show the potential for BLAnCA to identify different kinds of particulate matter based on their optical properties.

1. Introduction

Airborne particulate matter (PM) is present in the atmosphere in a variety of forms, which differ from each other in their origin, size, shape and composition (Boucher, 2015; Kolb and Worsnop, 2012; Seinfeld and Pandis, 2016). Atmospheric aerosols have a direct effect on the Earth's radiation budget, climate and ecosystems, by absorbing and scattering radiation (Bellouin et al., 2020), and several indirect effects, such as serving as condensation nuclei for warm and ice cloud formation (Engelhart et al., 2012) and promoting ocean productivity (Jickells and Moore, 2015). PM also has implications on health, due both to its small size, which makes aerosol particles inhalable, and to its chemical composition, which can render it toxic (Shiraiwa et al., 2017).

Among aerosol species, carbonaceous aerosols (CA) have the most relevant impact on the atmospheric radiative budget through their strong, broadband absorption (Chung et al., 2012). In particular, black carbon (BC) is defined as the black fraction of CA due to the wavelength independence of the imaginary part of its refractive index, which makes it a strong absorber across the entire visible range (Bond and Bergstrom, 2006; Moosmüller et al., 2009). Brown carbon (BrC) is a class of organic carbonaceous compounds which scatter light, and also absorb more selectively at shorter wavelengths (Andreae and Gelencsér, 2006). This gives BrC its characteristic brown-yellowish appearance. The main source of CA is combustion, with primary BrC being emitted from biomass combustion especially during the smoldering phase, while BC is emitted in varying proportions in all combustion processes (Yan et al., 2018). Secondary formation or aging of organic molecules can be other sources of BrC (Laskin et al., 2015).

Another aerosol category which absorbs solar radiation is mineral dust (MD). MD is the second most abundant PM species in the atmosphere (Knippertz and Stuut, 2014). It is mostly emitted by aeolian erosion on arid and semi-arid areas of the globe, but it is also has contributions from the resuspension of dust from human activities such as handling of resources, transport of goods and pasture (Kok et al., 2021; Scerri et al., 2023). Due to its mineralogical composition, in the solar spectrum MD interacts with light by scattering, and by absorption in relatively narrow spectral bands (Sokolik and Toon, 1999). While its mass specific absorption is at least one order of magnitude lower than for BC and BrC, its atmospheric load makes it relevant in the energy balance of the atmosphere (Caponi et al., 2017; Lafon et al., 2006; Nousiainen, 2009).

Generally, atmospheric aerosols contain species from several sources in varying proportions and at different stages of aging. The magnitude and spectral dependence of their light-absorption capabilities make it possible to distinguish them by their optical signature, and to perform source apportionment that allows the identification of their sources. A metric for the optical absorption behavior is the absorption Ångström exponent (AAE), defined as $AAE = -\ln(b_{abs}(\lambda_1)/b_{abs}(\lambda_2))/\ln(\lambda_1/\lambda_2)$, representing the spectral dependence of the aerosol absorption coefficient (b_{abs}) between two wavelengths of interest λ_1 and λ_2. The AAE value is linked to the PM composition as a function of its type, source, age and size distribution, with values close to 1 for BC and higher than 2 for BrC and MD (Caponi et al., 2017; Lack and Langridge, 2013) and is therefore a powerful tool to identify the light-absorbing components and the apportionment of their sources (Bernardoni et al., 2017a; Massabò et al., 2015; Sandradewi et al., 2008). To calculate the AAE of a PM species, it is necessary to measure its aerosol optical absorption coefficient at multiple wavelengths. A higher resolution can open the way to more sophisticated apportionment models by highlighting distinctive features in the absorption spectrum such as different curvatures or specific absorption bands. These features can be exploited to identify different aerosol species which could otherwise not be distinguished with a lower resolution.

Many instruments, both commercial and custom-made, have been developed over the years to accomplish this task. The aethalometer (Hansen et al., 1984) is an online instrument which measures attenuation of laser diode light as it passes through a filtering tape which is being progressively sampled with ambient aerosol, to obtain information on aerosol absorption. The instrument in its current version (Drinovec et al., 2015) measures at several wavelengths, ranging from the UV to the near-IR, and it is widely used although it suffers from some well-known artifacts which stem from its inability to measure the scattered light and to quantify the multiple scattering effect between filter matrix and aerosol (Coen et al., 2010; Virkkula et al., 2015). The correction of these artifacts requires knowledge of the scattering properties of the sampled aerosol, which must be obtained through independent techniques (e.g. Bernardoni et al., 2021).

The Multi Angle Absorption Photometer (MAAP), now discontinued, addressed this issue by measuring directly the light scattered by the sample at two backward angles, in addition to the transmitted light (Petzold and Schönlinner, 2004). This allows an estimation of the transmitted and backscattered light, which leads to a direct online determination of the aerosol b_{abs} through a data reduction scheme that takes into account the multiple scattering effects. The main drawback of the MAAP is that it works at only one wavelength, making it impossible to perform source apportionment studies based on measurements solely by this instrument.

An offline, custom instrument that moves forward from the MAAP is the Multi-Wavelength Absorbance Analyzer (MWAA), developed at the Physics Dept. of the University of Genoa (Massabò et al., 2013). The MWAA measures the absorption coefficient of PM samples at 5 wavelengths, ranging from the UV to the near-IR, following the MAAP multi-angle approach and data reduction scheme and giving its name to a new apportionment method (Bernardoni et al., 2017a; Massabò et al., 2015). Another multi-wavelength laboratory instrument based on the MAAP, but measuring the scattered light at high angular resolution, is the polar photometer PP_UNIMI (Vecchi et al., 2014, Bernardoni et al., 2017b). Both instruments were recently used to retrieve the multiple-scattering correction factors for the Aethalometer data (Bernardoni et al., 2021; Moschos et al., 2024; Yus-Díez et al., 2021).

As a further step forward in the measurement and source apportionment capability of the state-of-the-art instrumentation, we introduce here the new Broadband Light Analyzer of Complex Aerosol (BLAnCA), a custom laboratory instrument for offline light absorption measurements of PM samples. BLAnCA uses a white light source and a fiber-optic spectrometer to measure aerosol light absorption over a wide spectrum ranging from 375 to 1000 nm, with a 5 nm resolution (i.e. providing information at 125 wavelengths, whereas other currently existing instruments all work at less than 10 wavelengths). Furthermore, as already performed in PP_UniMI, BLAnCA measures the scattering profile at high angular resolution without relying on detectors placed at fixed angles. These features allow to identify the fine structure of the aerosol light absorption spectra that are indistinguishable with previous, lower-resolution devices, and to operate in principle on any kind of filters with no need of a-priori information on the shape of the sample phase function.

This paper presents a description of the instrument and its technical features, and the results of a characterization and validation campaign we carried out using an atmospheric simulation chamber. Examples of possible applications of BLAnCA to measure the absorption coefficient of a variety of laboratory-generated and ambient atmospheric aerosols are provided.

2. Instrument description

The schematic drawing and the photograph of the setup of BLAnCA are shown in Fig. 1. BLAnCA is assembled on an optical bench (STANDA optomechanics ltd, Lithuania) for stability and mounting convenience.

The light source is a broadband tungsten halogen lamp (Mighty Light Plus, Spectrolight Inc., USA), with a black-body emission spectrum peaked at approximately 680 nm. Two light transport configurations can be set up. In the standard configuration (Fig. 1), a light guide and a system of convex lenses of 2 cm of diameter (item c in Fig. 1) collimate the light onto the sample under analysis. The collimated light spot has a diameter of approximately 2 cm. A second configuration can be obtained by replacing the light guide with a fiber optic cable of 1000 μm diameter and an optical bandpass between 350 and 2500 nm (FC-IR1000-1, Avantes BV, The Netherlands) and the 2 cm lenses system with a smaller convex lens (COL-UV/VIS, Avantes BV, The Netherlands) whose focal point coincides with the end of the fiber cable, creating a collimated light diameter of approximately 0.6 cm. This configuration reduces the incident light intensity by 70 %, but it allows the analysis of samples where the aerosol is deposited on a smaller surface.

The spectrum of the incident light, in the standard configuration, is shown in Fig. 2.

Light transmitted through and scattered by the aerosol sample is carried to a CMOS spectrometer (AvaSpec ULS2048CL Avantes BV, The Netherlands) through a 200 μm diameter UV–VIS–NIR optical fiber cable (FC-UVIR-3, Avantes BV, The Netherlands). The spectral range of the spectrometer is 200–1100 nm, and its resolution is 5 nm. For our setup, the combination of the lamp emission spectrum, the efficiency of the light guide and of the fiber optic cable gives a reliable measurement range between 375 and 1000 nm. Outside of this range, the light reaching the spectrometer detecting element is comparable with the background noise and it is therefore impossible to extract meaningful

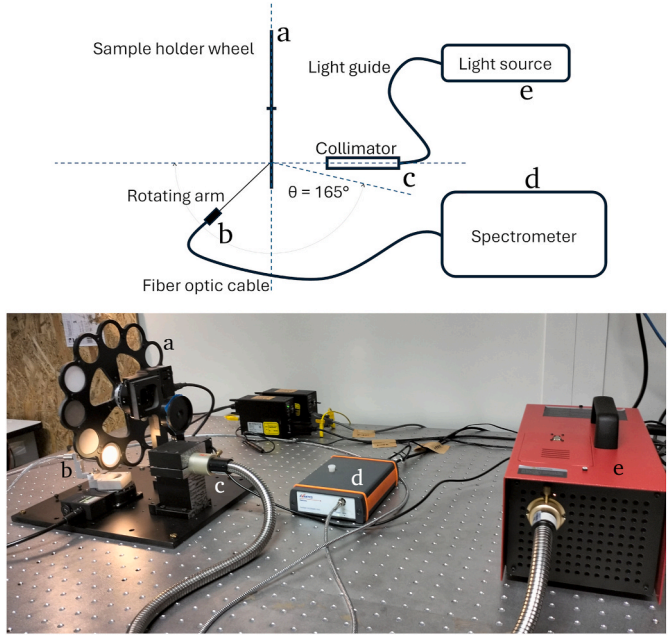

Fig. 1. The BLAnCA setup. Top: a scheme of the instrument. Bottom: a picture of the setup.

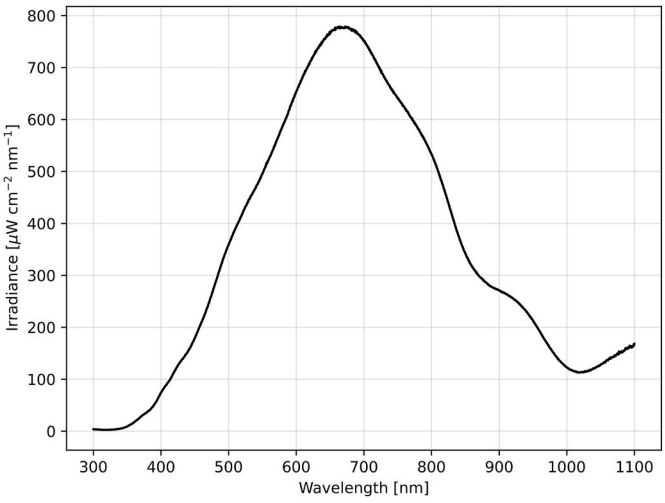

Fig. 2. Incident light spectrum. Note that the light guide and the collimating system of lenses have a lower transmittivity for long wavelengths, which are suppressed compared to a standard black-body emission curve.

information.

Aerosol samples are placed on a 12-position motorized filter holder wheel, indicated with a in Fig. 1, which enables the automatic sequential measurement of PM samples collected on circular filters. The fiber optic cable that feeds the spectrometer is mounted on a motorized arm (item b in Fig. 1), which rotates on the horizontal plane around the sample at a distance of 6 cm. The minimum rotation step is 0.1°, which allows a precise measurement of the light scattering profile of both blank and sampled filters, across the entire spectral range. Detailed description of the treatment of the raw data and the use of the scattering profile as input for the retrieval of aerosol absorption, is described in the supplementary material. For quartz fiber filters, we use an angular step of 5° since the scattering profile does not vary rapidly. For other types of filtering supports, the angular resolution can be adjusted according to the expected rate of change of the scattering profile (see the supplementary material). A custom LabView program controls the rotation of the filter holder wheel and the detector arm and acquires the data from the spectrometer via USB connection.

The absorbance of an aerosol sample, defined as $ABS = (1-\omega)\cdot\tau$ where ω is the single-scattering albedo of the aerosol-filter layer, and τ is its optical thickness, is determined by the radiative transfer model developed by Hänel (1987, 1994). This model necessitates precise measurements of light scattered in both the forward (A) and backward hemispheres (B) relative to the direction of travel of the light beam. In the case of BLAnCA, these hemispherical scattering measurements are directly obtained using the rotating arm. This setup allows for accurate detection of scattered light in both directions. The procedure for calculating ABS at a specific wavelength involves the following steps:

1) Data Acquisition: raw measurements of (A) and (B) are collected for both blank (particle-free) and particle-loaded filters. For quartz fiber filters, average values from blank filters can be utilized without compromising measurement accuracy.
2) Radiative Transfer Analysis: The collected data are input into the radiative transfer equations as outlined by Hänel (1987, 1994) and further refined by Petzold and Schönlinner (2004). These equations account for multiple scattering effects and interactions between the aerosol particles and the filter matrix.
3) Numerical Solution: By solving the radiative budget equations numerically (and with an assumption on the asymmetry parameter of the aerosol-filter layer), values for SSA and τ are derived. Subsequently, ABS is calculated using the initial equation.

From ABS, the aerosol absorption coefficient (b_{abs}, in Mm^{-1}) is obtained as $b_{abs} = ABS \cdot \frac{A}{V}$, where A is the area of the filter covered by deposited aerosol and V is the total volume of sampled air. A review of the data analysis scheme from raw measurements leading to the values of absorbance is presented in the supplementary material.

As pointed out by Valentini et al. (2021), the direct numerical integration of the scattering profiles makes the analysis model independent of assumptions on the scattering phase function shape, which are needed by other instruments (MAAP, MWAA). This allows the measurement of aerosol collected on every kind of non-absorbing filter medium.

3. Experimental methods

To characterize and validate the new instrument, we carried out an aerosol sampling campaign within an atmospheric simulation chamber (ASC) to produce PM samples on quartz filters, covering a wide range of loadings to compare the optical performance of BLAnCA against different benchmark instruments. We worked at the ChAMBRe (Chamber for Aerosol Modeling and Bio-aerosol Research) ASC (Vernocchi et al., 2023), installed at the Genoa division of the Italian National Institute of Nuclear Physics (INFN).

Artificial soot was produced by incomplete propane combustion in a Mini Inverted Soot Generator (MISG), with an air flow of 7 L min^{-1} and a fuel flow of 75 mL min^{-1}, according to the specifications in (Vernocchi et al., 2022). The injection time was varied, across the different experiments, between 30 s and 2 min, according to the desired soot concentration inside the chamber. The atmosphere inside the chamber was homogenized for 3 min by a fan placed on the bottom of the volume. After that, the aerosol was sampled on 47 mm quartz fiber filters (Pall Tissuquartz, 2500QAO-UP). We used a low-volume sampler (TCR Tecora, Italy) at different rates and sampling duration. The sampling variability, coupled with changes in soot concentration both within the same experiment (due to dilution induced by sampling) and across different experiments (due to different injection times), led to a very wide range of soot loading on the filters. A total of 30 samples were produced.

Another experiment was conducted in identical conditions as described above, with the additional deployment of three Photoacoustic Extinctiometers (PAX. Droplet Measurement Technologies, Inc., USA). The PAXs measure the aerosol absorption coefficient with an online technique where the aerosol particles are illuminated with pulsed laser and are consequently heated due to light absorption. Such (pulsed) heat acquired by the particles is rapidly transferred to the surrounding air and generates a compression wave which is then picked up by a microphone. Each of the three units works at a specific wavelength, namely 407, 532 and 870 nm. Each PAX unit had been calibrated following the procedure described in the user manual. During the experiments, the maximum b_{abs} measured by PAXs was less $1.2 \cdot 10^4$ Mm^{-1}, well within the linear upper limit reported in Nakayama et al. (2015); Zhang et al. (2021) (about $5 \cdot 10^4$ Mm^{-1}). More details on the instruments and their deployment in the ChAMBRe ASC can be found in Vernocchi et al. (2022). In this experiment, a total of 15 filter samples were produced.

Samples containing BrC aerosols were generated in an indoor combustion system that uses a tube furnace and a well characterized 9-m^3 Teflon environmental chamber (Smith et al., 2019) at the North Carolina A&T State University. Colophospermum mopane wood was placed in the tube furnace at an ignition temperature of 450 °C to induce controlled smoldered combustion (Moschos et al., 2024; Smith et al., 2020, McRee et al., 2025). The relative humidity inside the chamber system was 0 %. The resulting aerosol was sampled on 47 mm quartz filters.

Samples of mineral dust aerosols were generated from a natural soil from the Sonora desert (Arizona), previously sieved to 1 mm and dried in an oven for an hour at 100 °C, using a laboratory apparatus previously described in Baldo et al. (2020). A Buchner flask containing the dried soil sample was placed on a Retsch AS200 sieve shaker. The dry soil was shaken for a few minutes to mimic the natural process of emission. The generated dust aerosol particles were flowed through a cyclone impactor which selected only the particles with aerodynamic diameter less than 2.5 μm (PM2.5) and then sampled on pre-weighted 47 mm quartz filters by a pump operating at 16.7 L min-1.

Ambient aerosol samples were collected during a winter measurement campaign in Propata, a rural site in the Italian Apennine mountains (see for example Bernardoni et al., 2017a) and on the terrace of the Physics Dept. at the University of Genoa, Italy, an urban background site. In both campaigns a low-volume sampler (TCR-Tecora, Italy) was deployed to collect aerosol on quartz filters at a flow rate of 38.3 L min^{-1}, with an inlet impactor stage to select only the particles with aerodynamic diameter less than 10 μm (PM10). In Propata, the sampling time was 48 h; in Genoa it was 24 h.

A subset of 11 samples produced in ChAMBRe was analyzed with a thermo-optical EC/OC analyzer (Sunset Laboratory Inc.) to quantify the concentration of elemental carbon (EC) load on each filter. Elemental carbon is operationally defined as the fraction of the total carbonaceous PM present in a sample which does not combust at low temperatures in absence of oxygen (Bauer et al., 2009; Massabò and Prati, 2021). It is closely related to BC but the two quantities do not coincide (Petzold et al. 2013, and references therein). Considering the MISG combustion characteristics (Kazemimanesh et al., 2018; Vernocchi et al., 2022), we can assume that the analyzed ASC samples contain only BC as light absorbing species, and the EC quantified by the EC/OC analysis can be considered as a proxy for BC. The EC/TC ratio found with the EC/OC analysis was 0.7 for the samples presented in this work. Therefore, an EC/OC analysis performed on these filters allows to measure the mass of the absorbing species, and we expect a linear relationship between the surface mass concentration of the EC (c_{EC}) and the optical absorbance ABS. The proportionality coefficient is the mass absorption cross-section σ_{abs}, as expressed in:

$$ABS(\lambda) = 10^{-2}\, \sigma_{abs}(\lambda) \cdot c_{EC}, \quad (1)$$

where σ_{abs} is expressed in $m^2 g^{-1}$ and c_{EC} in μg cm^{-2}.

4. Measurements of spectral absorption

In this section, we present measurements conducted with the BLAnCA instrument. To illustrate the ability of the instrument to measure the spectral absorbance of three major light-absorbing aerosols (BC, BrC and mineral dust), we show the results from measurements conducted on samples generated in simplified conditions in the laboratory. Secondly, we resent the results obtained on samples collected in ambient conditions to demonstrate the ability of the instrument to identify the absorbing components of a complex aerosol mixture as found in the real atmosphere.

4.1. Laboratory experiments

The normalised light absorption spectra of propane soot, brown carbon and mineral dust generated in the laboratory are shown in Fig. 3.

The absorption of the propane soot sample (black dotted line) is consistent with the imaginary part of the refractive index of BC being independent of the wavelength (Bond and Bergstrom, 2006). The absorption Ångström exponent of this sample, calculated between the endpoints of the experimental range, is $AAE^{soot}_{375-1000} = 0.95 \pm 0.03$. The artificial BrC sample (red dashed line) evidences the typical absorption enhancement at low wavelengths that can be expected from this type of aerosol; its AAE is $AAE^{BrC}_{375-1000} = 2.33 \pm 0.03$. Finally, the Arizona desert dust sample (blue solid line) shows a more complex absorption behavior which can be split into three distinct sections, each of which has its own AAE: $AAE^{dust}_{375-450} = 2.67 \pm 0.16$, $AAE^{dust}_{450-590} = 3.65 \pm 0.11$ and $AAE^{dust}_{590-1000} = 3.27 \pm 0.06$. The overall AAE for the dust sample is

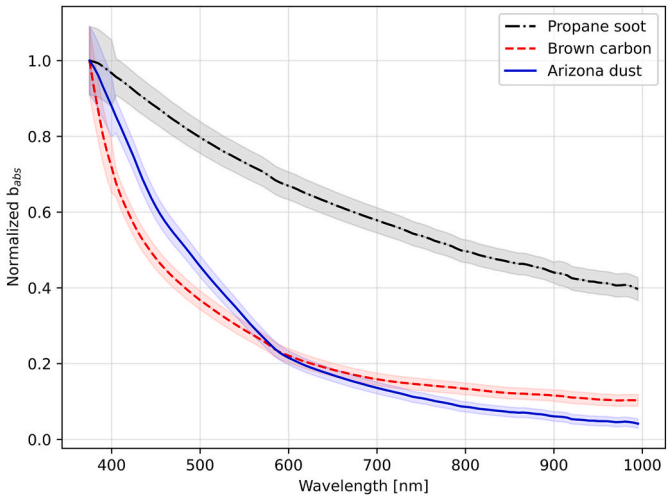

Fig. 3. Normalised absorption coefficient for the samples of propane soot, brown carbon biomass burning aerosols and mineral dust generated in the laboratory. Data (solid lines, with a 5 nm spectral resolution) are shown with their experimental uncertainty (shaded regions). (For interpretation of the references to colour in this figure legend, the reader is referred to the Web version of this article.)

$$AAE^{dust}_{375-1000} = 3.26 \pm 0.03.$$

4.2. Ambient samples

Fig. 4 shows the spectra of two ambient aerosol samples collected in Propata, a rural site in the Italian Apennine mountains.

The absorption of the rural aerosol sample (red dashed line) is due to carbonaceous aerosol from vehicular emission and local wood burning, the latter being the predominant fuel used for heating at the sampling location (Bernardoni et al., 2017b; Massabò et al., 2015). The absorption of this sample drops less rapidly than in the case of artificial BrC, shown in Fig. 3. This is because, while the ASC sample was BrC-dominated, the real sample is a complex mixture of aerosol from different sources and at different aging stages, of which wood burning aerosol is a primary component. The presence of BC in the sample increases the overall absorption, and in particular the relative value of absorption at longer wavelengths (i.e., decreasing the absorption Ångström exponent). The AAE for this sample is $AAE^{rural}_{375-1000} = 1.33 \pm 0.03$. It is worth noting that, from a qualitative perspective, the measured absorption spectrum of rural aerosol in Fig. 4 can be obtained from a superposition of a pure BC and a pure BrC absorption. In fact, the AAE for this sample is in between the values found for the artificial BC and BrC shown in Section 4.1. The absorption spectrum plotted in blue (solid line) in Fig. 4 shows an evident sharp bend at 600 nm, which is very similar to the behavior of the dust sample in Fig. 3, suggesting that the ambient sample was affected by the transport of mineral dust. This hypothesis is confirmed by the airmass back trajectory calculated using HYSPLIT, which shows winds coming from northern Africa (see the supplementary material). Subdivision of this absorption spectrum into three regions yields the following values for the absorption Ångström exponents: $AAE^{event}_{375-450} = 2.69 \pm 0.16$, $AAE^{event}_{450-590} = 4.29 \pm 0.11$ and $AAE^{event}_{590-1000} = 2.00 \pm 0.06$. The overall AAE for the dust sample is $AAE^{dust}_{375-1000} = 2.76 \pm 0.03$.

Fig. 5 shows the absorption of aerosol sampled on the terrace of the Physics Dept. at the University of Genoa, Italy, an urban background site.

The black dashed spectrum shows the average absorption of four filters collected during the campaign, excluding one sample whose spectrum is shown in the red solid line. The campaign average shows no significant spectral features, with an $AAE^{urban}_{375-1000} = 0.90 \pm 0.03$ which is indeed compatible with BC absorption shown in Fig. 3. An evident bump around 550 nm in the red solid absorption spectrum can be seen thanks to BLAnCA's high spectral resolution. On that day, construction works were going on near the department and some of the displaced soil and construction materials were sampled on the filter. During the rest of the campaign, no such events occurred, and therefore we attribute the absorption peak to such works. In this case, the absorption Ångström exponent is not a meaningful metric to evaluate the absorption characteristics of the sample.

5. Instrument characterization and validation

5.1. BLAnCA validation against the MWAA

In this section the performance of BLAnCA is evaluated by comparison with the MWAA, here considered as reference instrument. MWAA was validated against state-of-the-art instruments, such as the MAAP, and is therefore a good benchmark to evaluate the performance of BLAnCA (Massabò et al., 2013, 2015). The optical absorption coefficient

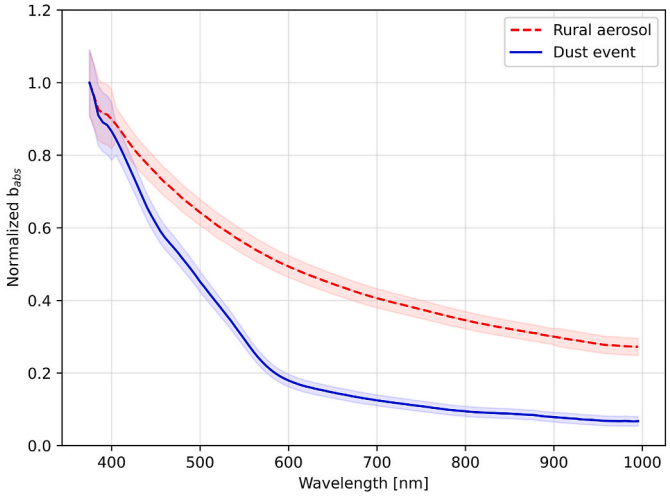

Fig. 4. Normalised absorption coefficient for ambient aerosol sampled during a campaign in a rural site in Propata, in the Italian Apennines. Data (solid lines, with 5 nm resolution) are shown with their experimental uncertainty (shaded regions).

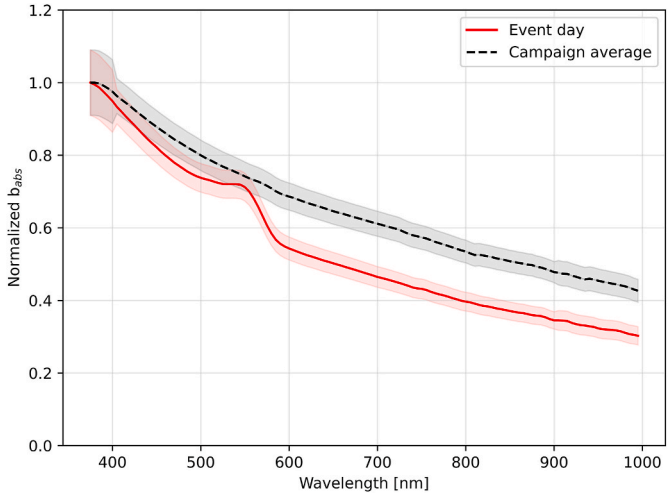

Fig. 5. Normalised absorption coefficient of aerosol sampled during a campaign at the Physics Dept. in Genova, an urban background site. Data (solid and dashed lines, with a 5 nm spectral resolution) are shown with their experimental uncertainty (shaded regions).

of the samples collected during the first ChAMBRe campaign is compared at the common wavelengths (375, 407, 532, 635 and 850 nm), performing a linear regression on the entire dataset (Fig. 6, left panel). The slope of the regression line on the entire dataset is **0.97**± **0.01**. The slope of the regression lines at each wavelength (Fig. 6, right panel) are between **0.96** ± **0.01** for λ = **407** nm and **0.99**± **0.01** for λ = **850** nm. In all cases, the R^2 of the regression is not lower than 0.99.

5.2. BLAnCA validation against the PAXs

Here we compare the performance of BLAnCA with the three Photoacoustic Extinctiometers. The optical absorption coefficient of the artificial soot samples collected during the second ChAMBRe campaign was measured offline with BLAnCA. The $\boldsymbol{b_{abs}}$ of each filter sample was compared with the average of the online PAX measurement, taken over the filter sampling period. The comparison was made at the three common wavelengths (405, 532 and 870 nm) performing a linear regression on the entire dataset and also for each wavelength separately (Fig. 7). The slope of the regression line on the entire dataset is **0.96** ± **0.01**. The slopes of the regression lines for the individual wavelengths are **0.95** ± **0.01** for 405 nm, **0.97** ± **0.01** for 532 nm and **0.96** ± **0.01** for 870 nm. The $\boldsymbol{R^2}$ of the regression is always higher than 0.98.

5.3. Uncertainty estimation

Several factors contribute to the uncertainty of an absorbance measurement performed by BLAnCA. First, the radiative transfer scheme that we follow to retrieve ABS needs a blank filter measurement as a reference. Since it is not always possible to measure a filter before PM sampling, the blank reference is often a different filter of the same batch. This leads to a wrong estimation of the power radiated in the forward and in the backward hemispheres by the aerosol. We estimated this uncertainty (δ_b) by measuring ABS for the same filter sample using five different blank references. Secondly, repeated measurements on the same sample give slightly different results due to changes in contour conditions, giving rise to hardware repeatability uncertainty (δ_h). Thirdly, we performed a sensitivity test to check how much a variation of 5 % in the raw spectrometer data propagates through the post-processing data analysis stages to the final ABS value; 5 % is a conservative estimate of the raw measurement statistical uncertainty, which rarely exceeds 1 %. This translated to the software sensitivity uncertainty (δ_s). Finally, when using a 5° angular resolution for the scattering profile measurement, the decreased resolution involves a slight drop in accuracy in ABS compared to the value obtained from a measurement at 1° resolution. This effect is captured in the angular uncertainty (δ_a). The uncertainty from each of the sources has a dependency on the wavelength. Therefore, the overall maximum relative uncertainty ($\delta^{\%}$) on a BLAnCA absorption measurement is given by:

$$\delta^{\%}(\lambda) = \delta_b^{\%}(\lambda) + \delta_h^{\%}(\lambda) + \delta_s^{\%}(\lambda) + \delta_a^{\%}(\lambda) = \begin{cases} 13\% \; if \; 375nm < \lambda < 400nm \\ 9\% \; if \; 400nm < \lambda < 900nm \\ 10\% \; if \; 900nm < \lambda < 1000nm \end{cases} \quad (2)$$

The values we obtained are, then, a conservative estimate of the measurement error. The uncertainty thus calculated is a sum of a statistical part and a systematic part, which contribute to each of the sources detailed above. The systematic uncertainty can be estimated from the comparison with the MWAA in section 4.1, assuming that the discrepancy between the BLAnCA and MWAA measurements can be attributed to systematics present in the setup. Therefore, we estimate the systematic contribution to relative uncertainty on a BLAnCA measurement as 4 %.

5.4. Evaluation of the limits of detection

Fig. 8 shows the scatter plot between ABS and $c_{EC,}$ and the corresponding regression lines at 375 and 1000 nm, chosen as they represent the lowest and highest boundaries of the experimental range, as well as 550 and 635 nm, commonly considered wavelengths for optical analysis of atmospheric aerosol. The linear regression between the measured ABS and c_{EC} is calculated to evaluate the spectrally resolved mass absorption cross-section of EC. For the propane soot produced in the ASC campaign, σ_{abs} is 7.5 ± 0.1 m^2g^{-1} at 635 nm, consistent with the literature values for black carbon (for example Bond and Bergstrom, 2006 and references therein), 11.5 ± 0.2 m^2g^{-1} at 375 nm, 8.7 ± 0.1 m^2g^{-1} at 550 nm and 4.7 ± 0.1 m^2g^{-1} at 1000 nm.

In addition to confirming the robustness of the measurements, this also gives an indication of the instrumental limits of detection. Since the scatter plots do not exhibit significant deviation from the linear correlation, we can estimate the limits of detection for BLAnCA. The lower limit of detection is $ABS_{min} \approx 0.06$, since 0.06 is the lowest ABS value that we measured at 1000 nm, and this value is still very well correlated with c_{EC}. We therefore conclude that the lower limit of detection is less than this conservative figure. With the same reasoning, we conservatively estimate the upper limit of detection $ABS_{max} \approx 2.3$ from the UV measurements. Our present dataset does not allow further exploration of the measurement limits, but these figures already indicate BLAnCA can measure PM across a broad range of loadings. The detection limits we found are similar to those of the MWAA, already presented in previous works, and approximately a factor 2 worse than the MAAP due to the more challenging evaluation of the blank response, which in BLAnCA is not measured simultaneously as it is with online instruments.

From the aforementioned considerations, from the minimum

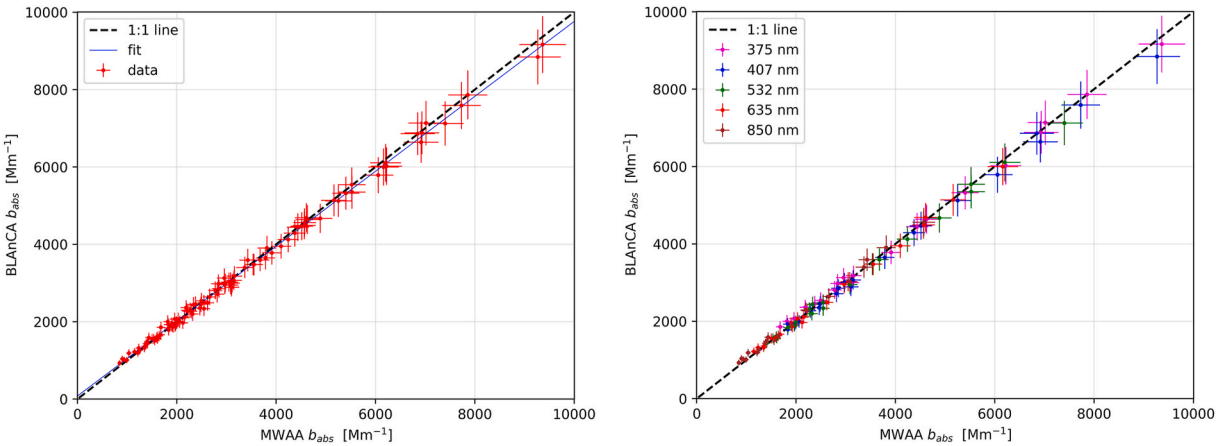

Fig. 6. Comparison of b_{abs} values measured by MWAA and BLAnCA, for all the wavelengths (left) and separated at the different λ s (rights).

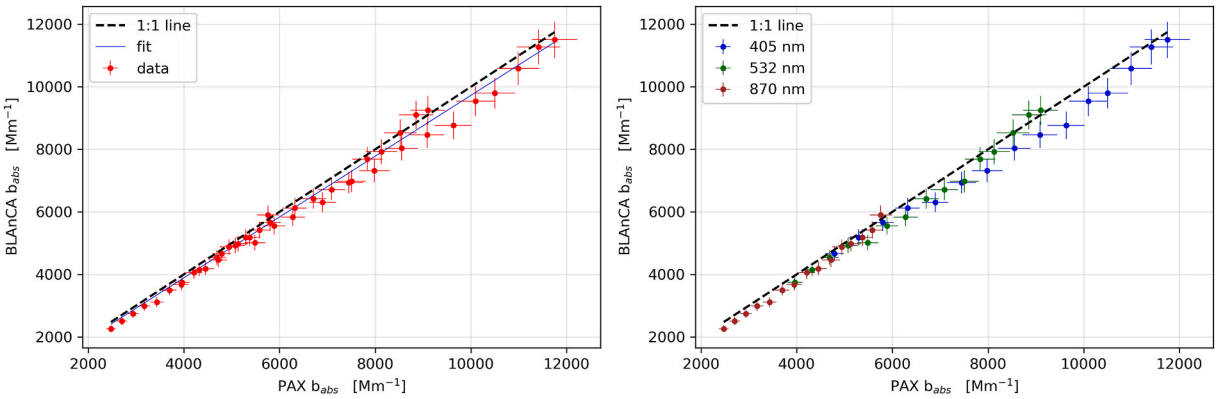

Fig. 7. Comparison of b_{abs} values measured by PAX and BLAnCA, for all the wavelengths (left) and separated at the different λ s (rights).

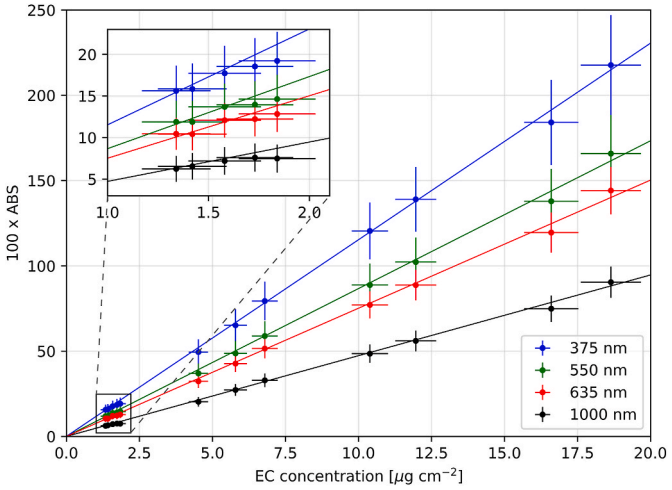

Fig. 8. Regression analysis to retrieve the σ_{abs} of soot generated with the Mini Inverted Soot Generator inside an atmospheric simulation chamber. The intercept of the regression lines is compatible with zero. The aerosol absorbance, on the y-axis, was measured with BLAnCA. The EC concentration on each filter, on the x-axis, was measured with a Sunset Laboratory EC/OC analyzer.

detectable ABS and σ_{abs} (1000 nm) we can evaluate the minimum equivalent black carbon (eBC) detectable surface concentration from equation (1) as $c_{eBC}^{min} \approx 1.3$ μg cm^{-2}. Considering a 24-h PM filter sampled at a flow rate of 38.3 L min^{-1} as per EU normative, this translates to a minimum detectable absorption coefficient of 1.20 Mm^{-1}, and a minimum detectable eBC concentration of $eBC^{min} \approx 250$ ng m^{-3}. With an EPA standard flow rate of 16.7 L min^{-1}, the minimum detectable absorption coefficient is 2.70 Mm^{-1} and the minimum detectable eBC concentration is 580 ng m^{-3}.

6. Conclusion

We have introduced BLAnCA, a new laboratory instrument for high spectral resolution measurements of the aerosol absorption coefficient. Thanks to the broad spectral range of the light source and of the spectrometer, BLAnCA can perform measurements from 375 to 1000 nm, with a resolution of 5 nm. This resolution allows to probe the fine structure of the absorption coefficient for a wide variety of aerosols sampled on filters. Indeed, the use of BLAnCA on laboratory-generated and ambient aerosol samples is successful in distinguishing the typical spectral dependence of black and brown carbon, and mineral dust aerosols. The spectra of mineral dust show a change in slope around 600 nm, differently from carbonaceous aerosols, for which the absorption curves are smoother, with variation (represented by the absorption Ångström exponent) and curvature depending on the type of carbonaceous aerosol present in the sample.

The performance of the instrument has been validated against a well-established instrument, the MWAA, obtaining a very good agreement at all the wavelengths at which the reference instrument operates. For black carbon, the maximum difference in the absorbance measured by the two instruments is 4 %, which we consider as an estimate of the systematic uncertainty on the BLAnCA measurement.

We have described the sources of experimental uncertainties of BLAnCA. The uncertainties have a dependency on wavelength; therefore, we identified three separate spectral regions where the relative error on the absorbance is different. We found a maximum relative uncertainty of 13 % in the 375–400 nm range, 9 % in the 400–900 nm range and 10 % in the 900–1000 nm range.

We have estimated the lower limit of detection of the instrument to be 1.20 Mm^{-1} (2.70 Mm^{-1}), corresponding to 250 ng m^{-3} (580 ng m^{-3}) for 24 h filters sampled with a standard EU (EPA) air flow. This limit of detection indeed allows the measurement of filters with a wide range of aerosol load, including those sampled in rural areas or otherwise sites that are only slightly polluted. Moreover, we emphasize that the primary function of BLAnCA is the offline measurement of the optical behavior of particulate matter and the study of physical properties of different types of aerosols, and not the determination of atmospheric PM concentration.

The high spectral resolution of the new instruments can be exploited to measure climate relevant physical properties of the PM, and for aerosol source apportionment with existing optical apportionment models, such as the MWAA model (Isolabella et al., 2024; Massabò et al., 2015). However, to fully utilize the amount of data provided by BLAnCA, a new optical apportionment model will be developed, with the aim of distinguishing more aerosol sources and components based on their optical signature.

CRediT authorship contribution statement

Tommaso Isolabella: Writing – original draft, Validation, Methodology, Investigation, Formal analysis, Data curation, Conceptualization. **Marco Brunoldi:** Writing – review & editing, Investigation. **Federico Mazzei:** Writing – review & editing, Investigation. **Franco Parodi:** Methodology. **Paolo Prati:** Writing – review & editing, Investigation, Funding acquisition, Formal analysis, Conceptualization. **Virginia Vernocchi:** Writing – review & editing, Investigation. **Vera Bernardoni:** Writing – review & editing, Validation. **Gianluigi Valli:** Writing – review & editing, Validation. **Roberta Vecchi:** Writing – review & editing, Validation. **Paola Formenti:** Writing – review & editing, Methodology, Investigation. **Clarissa Baldo:** Writing – review & editing, Methodology, Investigation. **Mathieu Cazaunau:** Writing – review & editing, Methodology, Investigation. **Vaios Moschos:** Writing – review & editing, Investigation. **Solomon Bililign:** Writing – review & editing,

Investigation. **Marc N. Fiddler:** Writing – review & editing, Investigation. **Dario Massabò:** Writing – review & editing, Investigation, Funding acquisition, Formal analysis, Conceptualization.

Funding

This work was supported by the Italian Ministry of the University (MUR) with the PRIN2017 grant for the RHAPS project [grant number: 2017MSN7M8], by the National Institute for Nuclear Physics (INFN) through the CSN5-ISPIRA and HARDLIFE experiments, the PNRR MUR - M4C2 – Investimento 1.3 - "Multi-Risk science for resilient commUnities undeR a changiNg climate (RETURN)" PE00000005 CUP HUB B63D22000670006, and IR0000032–ITINERIS, Italian Integrated Environmental Research Infrastructures System (D.D. n. 130/2022 - CUP B53C22002150006) funded by the EU (Next Generation EU PNRR, Mission 4 "Education and Research", Component 2 "From research to business", Investment Line 3.1, "Fund for the realisation of an integrated system of research and innovation infrastructures"). This work was partially supported by the "PHC GALILEE" programme (project number: 50397UA), funded by the French Ministry for Europe and Foreign Affairs, the French Ministry for Higher Education and Research and the Italian Ministero dell'Università e della Ricerca (MUR)" and the project Galileo 2024 – G24-170 "Progressi metrologici sulle proprietà ottiche degli aerosol desertici". This work was supported by the European Union under the Next generation EU program project number 2022CH87SA - IT-BEST. V.M. acknowledges support by the Swiss National Science Foundation (SNSF) under the Postdoc.Mobility Fellowship grant P500PN_210745. V.M, S.B and M.N.F acknowledge the support by the United States National Science Foundation (NSF) through the Atmospheric & Geospace Sciences (AGS) Division Grant # 2100708.

Declaration of competing interest

The authors declare that they have no known competing financial interests or personal relationships that could have appeared to influence the work reported in this paper.

Acknowledgments

We are indebted to the personnel of the INFN Genoa mechanical workshop for their support in developing custom instrumentation.

Appendix A. Supplementary data

Supplementary data to this article can be found online at https://doi.org/10.1016/j.atmosenv.2025.121341.

Data availability

Data will be made available on request.

References

Andreae, M.O., Gelencsér, A., 2006. Black carbon or brown carbon? The nature of light-absorbing carbonaceous aerosols. Atmos. Chem. Phys. 6, 3131–3148. https://doi.org/10.5194/acp-6-3131-2006.

Baldo, C., Formenti, P., Nowak, S., Chevaillier, S., Cazaunau, M., Pangui, E., Di Biagio, C., Doussin, J.-F., Ignatyev, K., Dagsson-Waldhauserova, P., Arnalds, O., MacKenzie, A.R., Shi, Z., 2020. Distinct chemical and mineralogical composition of Icelandic dust compared to northern African and Asian dust. Atmos. Chem. Phys. 20, 13521–13539. https://doi.org/10.5194/acp-20-13521-2020.

Bauer, J.J., Yu, X., Cary, R., Laulainen, N., Berkowitz, C., 2009. Characterization of the sunset semi-continuous carbon aerosol analyzer. J. Air Waste Manag. Assoc. 59, 826–833. https://doi.org/10.3155/1047-3289.59.7.826.

Bellouin, N., Quaas, J., Gryspeerdt, E., Kinne, S., Stier, P., Watson-Parris, D., Boucher, O., et al., 2020. Bounding global aerosol radiative forcing of climate change. Rev. Geophys. (1985) 58. https://doi.org/10.1029/2019RG000660.

Bernardoni, V., Pileci, R.E., Caponi, L., Massabò, D., 2017a. The multi-wavelength absorption analyzer (MWAA) model as a tool for source and component apportionment based on aerosol absorption properties: application to samples collected in different environments. Atmosphere 8, 218. https://doi.org/10.3390/atmos8110218.

Bernardoni, V., Valli, G., Vecchi, R., 2017b. Set-up of a multi wavelength polar photometer for off-line absorption coefficient measurements on 1-h resolved aerosol samples. J. Aerosol Sci. 107, 84–93. https://doi.org/10.1016/j.jaerosci.2017.02.009.

Bernardoni, V., Ferrero, L., Bolzacchini, E., Forello, A.C., Gregorič, A., Massabò, D., Močnik, G., Prati, P., Rigler, M., Santagostini, L., Soldan, F., Valentini, S., Valli, G., Vecchi, R., 2021. Determination of Aethalometer multiple-scattering enhancement parameters and impact on source apportionment during the winter 2017/18 EMEP/ACTRIS/COLOSSAL campaign in Milan. Atmos. Meas. Tech. 14, 2919–2940. https://doi.org/10.5194/amt-14-2919-2021.

Bond, T.C., Bergstrom, R.W., 2006. Light absorption by carbonaceous particles: an investigative review. Aerosol. Sci. Technol. 40, 27–67. https://doi.org/10.1080/02786820500421521.

Boucher, O., 2015. Atmospheric Aerosols. Springer, Netherlands.

Caponi, L., Formenti, P., Massabó, D., Di Biagio, C., Cazaunau, M., Pangui, E., Chevaillier, S., Landrot, G., Andreae, M.O., Kandler, K., et al., 2017. Spectral-and size-resolved mass absorption efficiency of mineral dust aerosols in the shortwave spectrum: a simulation chamber study. Atmos. Chem. Phys. 17, 7175–7191. https://doi.org/10.5194/acp-17-7175-2017.

Chung, C.E., Ramanathan, V., Decremer, D., 2012. Observationally constrained estimates of carbonaceous aerosol radiative forcing. Proc. Natl. Acad. Sci. 109, 11624–11629. https://doi.org/10.1073/pnas.1203707109.

Coen, M. Collaud, Weingartner, E., Apituley, A., Ceburnis, D., Fierz-Schmidhauser, R., Flentje, H., Henzing, J.S., Jennings, S.G., Moerman, M., Petzold, A., et al., 2010. Minimizing light absorption measurement artifacts of the Aethalometer: evaluation of five correction algorithms. Atmos. Meas. Tech. 3, 457–474. https://doi.org/10.5194/amt-3-457-2010.

Drinovec, L., Močnik, G., Zotter, P., Prévôt, A.S.H., Ruckstuhl, C., Coz, E., Rupakheti, M., Sciare, J., Müller, T., Wiedensohler, A., Hansen, A.D.A., 2015. The "dual-spot" Aethalometer: an improved measurement of aerosol black carbon with real-time loading compensation. Atmos. Meas. Tech. 8, 1965–1979. https://doi.org/10.5194/amt-8-1965-2015.

Engelhart, G.J., Hennigan, C.J., Miracolo, M.A., Robinson, A.L., Pandis, S.N., 2012. Cloud condensation nuclei activity of fresh primary and aged biomass burning aerosol. Atmos. Chem. Phys. 12, 7285–7293. https://doi.org/10.5194/acp-12-7285-2012.

Hänel, G., 1987. Radiation budget of the boundary layer: Part II. Simultaneous measurement of mean solar volume absorption and extinction coefficients of particles. Beiträge zur Physik der Atmosphäre 60, 241–247.

Hänel, G., 1994. Optical properties of atmospheric particles: complete parameter sets obtained through polar photometry and an improved inversion technique. Appl. Opt. 33, 7187–7199. https://doi.org/10.1364/AO.33.007187.

Hansen, A.D.A., Rosen, H., Novakov, T., 1984. The aethalometer—an instrument for the real-time measurement of optical absorption by aerosol particles. Sci. Total Environ. 36, 191–196. https://doi.org/10.1016/0048-9697(84)90265-1.

Isolabella, T., Bernardoni, V., Bigi, A., Brunoldi, M., Mazzei, F., Parodi, F., Prati, P., Vernocchi, V., Massabò, D., 2024. A new software toolkit for optical apportionment of carbonaceous aerosol. Atmos. Meas. Tech. 17, 1363–1373. https://doi.org/10.5194/amt-17-1363-2024.

Jickells, T., Moore, C.M., 2015. The importance of atmospheric deposition for ocean productivity. Annu. Rev. Ecol. Evol. Syst. 46, 481–501. https://doi.org/10.1146/annurev-ecolsys-112414-054118.

Kazemimanesh, M., Moallemi, A., Thomson, K., Smallwood, G., Lobo, P., Olfert, J.S., 2018. A novel miniature inverted-flame burner for the generation of soot nanoparticles. Aerosol. Sci. Technol. 53 (2), 184–195. https://doi.org/10.1080/02786826.2018.1556774.

Knippertz, P., Stuut, J.-B., 2014. Mineral Dust. Springer, Netherlands, Dordrecht. https://doi.org/10.1007/978-94-017-8978-3.

Kok, J.F., Adebiyi, A.A., Albani, S., Balkanski, Y., Checa-Garcia, R., Chin, M., Colarco, P. R., Hamilton, D.S., Huang, Y., Ito, A., Klose, M., Li, L., Mahowald, N.M., Miller, R.L., Obiso, V., Pérez García-Pando, C., Rocha-Lima, A., Wan, J.S., 2021. Contribution of the world's main dust source regions to the global cycle of desert dust. Atmos. Chem. Phys. 21, 8169–8193. https://doi.org/10.5194/acp-21-8169-2021.

Kolb, C.E., Worsnop, D.R., 2012. Chemistry and composition of atmospheric aerosol particles. Annu. Rev. Phys. Chem. 63, 471–491. https://doi.org/10.1146/annurev-physchem-032511-143706.

Lack, D.A., Langridge, J.M., 2013. On the attribution of black and brown carbon light absorption using the Ångström exponent. Atmos. Chem. Phys. 13, 10535–10543. https://doi.org/10.5194/acp-13-10535-2013.

Lafon, S., Sokolik, I.N., Rajot, J.L., Caquineau, S., Gaudichet, A., 2006. Characterization of iron oxides in mineral dust aerosols: implications for light absorption. J. Geophys. Res. Atmos. 111. https://doi.org/10.1029/2005JD007016.

Laskin, A., Laskin, J., Nizkorodov, S.A., 2015. Chemistry of atmospheric Brown carbon. Chem. Rev. 115 (10), 4335–4382. https://doi.org/10.1021/cr5006167.

Massabò, D., Prati, P., 2021. An overview of optical and thermal methods for the characterization of carbonaceous aerosol. La Rivista del Nuovo Cimento 44, 145–192. https://doi.org/10.1007/s40766-021-00017-8.

Massabò, D., Bernardoni, V., Bove, M.C., Brunengo, A., Cuccia, E., Piazzalunga, A., Prati, P., Valli, G., Vecchi, R., 2013. A multi-wavelength optical set-up for the characterization of carbonaceous particulate matter. J. Aerosol Sci. 60, 34–46. https://doi.org/10.1016/j.jaerosci.2013.02.006.

Massabò, D., Caponi, L., Bernardoni, V., Bove, M.C., Brotto, P., Calzolai, G., Cassola, F., Chiari, M., Fedi, M.E., Fermo, P., et al., 2015. Multi-wavelength optical

determination of black and brown carbon in atmospheric aerosols. Atmos. Environ. 108, 1–12. https://doi.org/10.1016/j.atmosenv.2015.02.058.
McRee, M.M., Moschos, V., Fiddler, M.N., Massabò, D., Surratt, J.D., Bililign, S., 2025. Influence of relative humidity and aging on the optical properties of organic aerosols from burning African biomass fuels. Aerosol. Sci. Technol. 59 (5), 544–566. https://doi.org/10.1080/02786826.2024.2412652.
Moosmüller, H., Chakrabarty, R.K., Arnott, W.P., 2009. Aerosol light absorption and its measurement: a review. J. Quant. Spectrosc. Radiat. Transf. 110, 844–878. https://doi.org/10.1016/j.jqsrt.2009.02.035.
Moschos, V., Christensen, C., Mouton, M., Fiddler, M.N., Isolabella, T., Mazzei, F., Massabò, D., Turpin, B.J., Bililign, S., Surratt, J.D., 2024. Quantifying the light-absorption properties and molecular composition of Brown carbon aerosol from Sub-Saharan African biomass combustion. Environ. Sci. Technol. 58, 4268–4280. https://doi.org/10.1021/acs.est.3c09378.
Nakayama, T., Suzuki, H., Kagamitani, S., Ikeda, Y., Uchiyama, A., Matsumi, Y., 2015. Characterization of a three wavelength photoacoustic soot spectrometer (PASS-3) and a photoacoustic extinctiometer (PAX). J. Meteorol. Soc. Jpn. 93 (2). https://doi.org/10.2151/jmsj.2015-016, 285:308.
Nousiainen, T., 2009. Optical modeling of mineral dust particles: a review. J. Quant. Spectrosc. Radiat. Transf. 110, 1261–1279. https://doi.org/10.1016/j.jqsrt.2009.03.002.
Petzold, A., Schönlinner, M., 2004. Multi-angle absorption photometry—a new method for the measurement of aerosol light absorption and atmospheric black carbon. J. Aerosol Sci. 35, 421–441. https://doi.org/10.1016/j.jaerosci.2003.09.005.
Sandradewi, J., Prévôt, A.S.H., Szidat, S., Perron, N., Rami Alfarra, M., Lanz, V.A., Weingartner, E., Baltensperger, U.R.S., 2008. Using aerosol light absorption measurements for the quantitative determination of wood burning and traffic emission contributions to particulate matter. Environ. Sci. Technol. 42, 3316–3323. https://doi.org/10.1021/es702253m.
Scerri, M.M., Weinbruch, S., Delmaire, G., Mercieca, N., Nolle, M., Prati, P., Massabò, D., 2023. Exhaust and non-exhaust contributions from road transport to PM10 at a southern European traffic site. Environ. Pollut. 316, 120569. https://doi.org/10.1016/j.envpol.2022.120569.
Seinfeld, J.H., Pandis, S.N., 2016. Atmospheric Chemistry and Physics: from Air Pollution to Climate Change. John Wiley & Sons.
Shiraiwa, M., Ueda, K., Pozzer, A., Lammel, G., Kampf, C.J., Fushimi, A., Enami, S., Arangio, A.M., Fröhlich-Nowoisky, J., Fujitani, Y., et al., 2017. Aerosol health effects from molecular to global scales. Environ. Sci. Technol. 51, 13545–13567. https://doi.org/10.1021/acs.est.7b04417.
Smith, D.M., Fiddler, M.N., Sexton, K.G., Bililign, S., 2019. Construction and characterization of an indoor smog chamber for measuring the optical and physicochemical properties of aging biomass burning aerosols. Aerosol Air Qual. Res. 19, 467–483. https://doi.org/10.4209/aaqr.2018.06.0243.
Smith, D.M., Fiddler, M.N., Pokhrel, R.P., Bililign, S., 2020. Laboratory studies of fresh and aged biomass burning aerosol emitted from east African biomass fuels – Part 1: optical properties, Atmos. Chem. Phys. 20, 10149–10168. https://doi.org/10.5194/acp-20-10149-2020.
Sokolik, I.N., Toon, O.B., 1999. Incorporation of mineralogical composition into models of the radiative properties of mineral aerosol from UV to IR wavelengths. J. Geophys. Res. Atmos. 104, 9423–9444. https://doi.org/10.1029/1998JD200048.
Valentini, S., Bernardoni, V., Bolzacchini, E., Ciniglia, D., Ferrero, L., Forello, A.C., Massabó, D., Pandolfi, M., Prati, P., Soldan, F., Valli, G., Yus-Diéz, J., Alastuey, A., Vecchi, R., 2021. Applicability of benchtop multi-wavelength polar photometers to off-line measurements of the Multi-Angle Absorption Photometer (MAAP) samples. J. Aerosol Sci. 152, 105701. https://doi.org/10.1016/j.jaerosci.2020.105701.
Vernocchi, V., Brunoldi, M., Danelli, S.G., Parodi, F., Prati, P., Massabò, D., 2022. Characterization of soot produced by the mini inverted soot generator with an atmospheric simulation chamber. Atmos. Meas. Tech. 15, 2159–2175. https://doi.org/10.5194/amt-15-2159-2022.
Vecchi, R., Bernardoni, V., Paganelli, C., Valli, G., 2014. A filter-based light-absorption measurement with polar photometer: Effects of sampling artefacts from organic carbon. Journal of Aerosol Science 70, 15–25. https://doi.org/10.1016/j.jaerosci.2013.12.012.
Vernocchi, V., Abd El, E., Brunoldi, M., Danelli, S.G., Gatta, E., Isolabella, T., Mazzei, F., Parodi, F., Prati, P., Massabò, D., 2023. Airborne bacteria viability and air quality: a protocol to quantitatively investigate the possible correlation by an atmospheric simulation chamber. Atmos. Meas. Tech. 16, 5479–5493. https://doi.org/10.5194/amt-16-5479-2023.
Virkkula, A., Chi, X., Ding, A., Shen, Y., Nie, W., Qi, X., Zheng, L., Huang, X., Xie, Y., Wang, J., Petäjä, T., et al., 2015. On the interpretation of the loading correction of the aethalometer. Atmos. Meas. Tech. 8, 4415–4427. https://doi.org/10.5194/amt-8-4415-2015.
Yan, J., Wang, X., Gong, P., Wang, C., Cong, Z., 2018. Review of brown carbon aerosols: recent progress and perspectives. Sci. Total Environ. 634, 1475–1485. https://doi.org/10.1016/j.scitotenv.2018.04.083.
Yus-Díez, J., Bernardoni, V., Močnik, G., Alastuey, A., Ciniglia, D., Ivančič, M., Querol, X., Perez, N., Reche, C., Rigler, M., Vecchi, R., Valentini, S., Pandolfi, M., 2021. Determination of the multiple-scattering correction factor and its cross-sensitivity to scattering and wavelength dependence for different AE33 Aethalometer filter tapes: a multi-instrumental approach. Atmos. Meas. Tech. 14, 6335–6355. https://doi.org/10.5194/amt-14-6335-2021.
Zhang, J., Chen, J., Wang, M., Su, M., Zhou, W., Varma, R., Lou, S., 2021. Intercomparison of photoacoustic and cavity attenuated phase shift instruments: laboratory calibration and field measurements. Geosci. Instrum. Method. Data Syst. 10, 245–255. https://doi.org/10.5194/gi-10-245-2021.